Energy 148 (2018) 1140–1152

Contents lists available at ScienceDirect

Energy

journal homepage: www.elsevier.com/locate/energy

Techno-economic assessment of Joule-Brayton cycle architectures for heat to power conversion from high-grade heat sources using CO_2 in the supercritical state

Matteo Marchionni, Giuseppe Bianchi*, Savvas A. Tassou

Institute of Energy Futures, Centre for Sustainable Energy Use in Food Chains, Brunel University London, Uxbridge, Middlesex UB8 3PH, UK

ARTICLE INFO

Article history:
Received 27 October 2017
Received in revised form
24 January 2018
Accepted 2 February 2018
Available online 4 February 2018

Keywords:
Supercritical CO_2 power cycle
Waste heat recovery
Techno-economic comparison
Thermodynamic analysis
Exergy analysis
High-grade heat to power conversion

ABSTRACT

Bottoming thermodynamic power cycles using supercritical carbon dioxide (sCO_2) are a promising technology to exploit high temperature waste heat sources. CO_2 is a non-flammable and thermally stable compound, and due to its favourable thermophysical properties in the supercritical state, it can achieve high cycle efficiencies and a substantial reduction in size and cost compared to alternative heat to power conversion technologies. Eight variants of the sCO_2 Joule-Brayton cycle have been investigated. Cycle modelling and sensitivity analysis identified the Turbine Inlet Temperature (TIT) as the most influencing variable on cycle performance, with reference to a heat source gas flow rate of 1.0 kg/s and 650 °C. Energy, exergy and cost metrics for different cycle layouts have been compared for varying TIT in the range between 250 °C and 600 °C. The analysis has shown that the most complex sCO_2 cycle configurations lead to higher overall efficiency and net power output but also to higher investment costs. Conversely, more basic architectures, such as the simple regenerative cycle, with a TIT of 425 °C, would be able to achieve an overall efficiency of 25.2%, power output of 93.7 kW_e and a payback period of less than two years.

1. Introduction

Nowadays primary energy sources still rely on fossil fuels, whose shortage and environmental impact pose serious concerns on their usage in the short term future. To reduce the fossil dependency, the use of renewable sources should be supplemented by an increase of energy efficiency in the existing power generation and industrial systems. In fact, it has been estimated that the 63% of the overall global energy consumption is lost after combustion and heat transfer processes for an absolute energy waste equal to 14.16 PWh [1]. In most of the cases, the wasted energy occurs as heat streams in the form of effluents or exhausts at low (<100 °C), medium (100–300 °C) and high temperature levels (>300 °C) [2]. Hence, their recovery and reuse would likely be some of the most effective opportunities to enhance the sustainability of current energy and manufacturing processes.

Among the Waste Heat Recovery (WHR) technologies, heat to power conversion systems benefit of attractive economic figures and flexibility in the reuse of the recovered heat. Furthermore, depending on the temperature range at which the heat is available, several approaches can be adopted. For medium temperature ranges, Organic Rankine Cycle (ORC) systems proved to be a successful technological solution especially for large scale applications [3]. In the last decade, plenty of academic and industrial research has been also carried out to develop mid and small-scale ORC systems [4]. Nevertheless, for high temperature waste heat sources, the ORC technology appears to be less attractive because of the lower chemical stability and high flammability of the working fluids to employ in such applications. In contrast, bottoming thermodynamic cycles based on supercritical carbon dioxide (sCO_2) could be a promising alternative to harvest the high temperature waste heat potential, which on a global scale accounts for 9.4% of the overall amount of energy rejected into the environment [5].

The main benefit of the sCO_2 technology derives from the distinct chemical and physical properties that CO_2 assumes in the supercritical state, and particularly near the critical point (30.98 °C, 73.8 bar). In these operating conditions, CO_2 presents very high density, isobaric thermal capacity and isothermal compressibility that allow to substantially reduce the compression work, and consequently, to increase the net power output and the overall efficiency of the bottoming thermodynamic cycle that, unlike ORC

* Corresponding author.
E-mail address: giuseppe.bianchi@brunel.ac.uk (G. Bianchi).

https://doi.org/10.1016/j.energy.2018.02.005

systems, is based on a Joule-Brayton one [6].

As concerns the application potential, the attractiveness of this technology increases when the heat is rejected at temperatures which are above 400 °C. In fact, in this range, the sCO_2 Brayton cycle presents numerous benefits with respect to conventional Rankine systems since CO_2 is not flammable and more chemically stable at higher temperatures than organic fluids [7]. Moreover, it is less expensive and more eco-friendly, since it is a non-toxic compound with a unitary Global Warming Potential and a null Ozone Depletion one.

Compared with the steam Rankine Cycle, the sCO_2 Joule-Brayton one allows to achieve better efficiencies at lower temperatures [8,9] and it presents lower capital and operational costs since sCO_2 is several times denser than steam. This feature allows to operate with compact and simple components which would also require less maintenance [10]. Furthermore, with respect to the Rankine technologies, the sCO_2 one allows a better thermal matching between the temperature glides of working fluid and hot source and, in turn, to achieve a higher 2nd law (exergy) efficiency, i.e. a better heat utilization [11].

For these reasons, simplified or more complex configurations of sCO_2 power cycles are being considered for high-grade heat to power conversion application including next generation nuclear and fossil fuel power generation (500–1000 MW_e) [12,13], modular nuclear power generation (300 MW_e) [14–17], solar thermal power generation (10–100 MW_e) [18–25], shipboard propulsion, geothermal, oxy-combustion and house power (1–100 MW_e) [26–35], and industrial scale waste heat recovery (1–10 MW_e) [36,37].

The technical feasibility of such systems has been so far assessed mostly at a theoretical level, and it has been focused on cycle analyses of large power plants. In particular, Kacludis et al. [38] reported an overview of several possible WHR applications for a 7.5 MW_e condensing simple recuperated sCO_2 power cycle, also known as sCO_2 Rankine cycle. Mondal et al. [39] presented a sCO_2 Brayton cycle with multi-stage intercooled compression considering as waste heat source a flue gas stream at 180 °C. The number of compression stages together with the key parameters of the cycle have been optimized in order to achieve the best cycle 1st and 2nd laws efficiency. In the analysis however, optimistic values for the efficiencies of the several components have been assumed. Moreover in the temperature range considered, other heat to power conversion systems can achieve competitive performance at lower costs.

Mohagheghi et al. [40] optimized simple regenerated and recompressed layouts recovering heat from a 100 kg/s exhaust stream. The results showed that adopting the re-compression layout, which guarantees the maximization of the overall cycle efficiency, does not provide benefits in terms of net power output, which is much more relevant for energy recovery systems. A 100 MW_e re-compression sCO_2 power unit for nuclear applications has been analyzed also by Moisseytsev et al. [41], where the impact deriving from the introduction of re-heating and intercooling was evaluated in terms of efficiency and net power output. What has been found is that the small increase of performance does not justify the resulting increased plant complexity.

A further analysis of sCO_2 cycle layouts for nuclear applications has been carried out by Kulhánek et al. [42], where the simple Brayton cycle has been compared to the re-compression, pre-compression, split expansion, partial cooling and partial cooling with improved regeneration cycles. From the results did not emerge a privileged scheme, since the performance of each configuration are too much affected by the particular operating conditions.

Even more complex configurations are reported by Ahn et al. and Crespi et al. [43,44], while Kimzey [45] presented several schemes to maximize the heat recovered and to achieve the best thermal matching inside the sCO_2 recuperators. The sCO_2 systems have been considered as bottoming units for a Siemens H class and a GE LM6000-PH combined cycles with a power scale of 195 MW_e and 14 MW_e respectively. Kim et al. [46] compared the simple regenerated, the pre-heating and a cascade sCO_2 Rankine cycle for the recovery of the heat rejected by a 25 MW_e gas turbine. The pre-heating architecture was found to be the one with the highest net power output. However, the sCO_2 Rankine cycle technology requires a larger heat source and heat sink capacity as well as the use of CO_2 pumps, which nowadays cannot fulfill high reliability requirements.

An extensive analysis of various simple and cascading sCO_2 Brayton cycle layouts as bottoming system of a gas turbine power plant has instead been carried out by Cho et al. [47]. In this work the performance of seven architectures (intercooling, cascading, and split concept cycles) were compared with the ones of a Rankine steam power unit. The results showed that high complex configurations did not provide a net power output greater than the reference Rankine cycle even though re-heating and pre-compression positively affected the performance of the sCO_2 bottoming unit. Nevertheless, the power scale of the system analyzed was higher than 100 MW_e, a range in which steam power plants can achieve very high efficiency thanks to their mature Technological Readiness Level (TRL).

A more pragmatic study has been reported by Wright et al. [48], regarding a thermo-economic comparison between four different cycle layouts (single-recuperated, a cascade cycle, a dual-recuperated cycle, and a pre-heating cycle) as bottoming power unit for a gas turbine power plant. The results showed that the pre-heating cycle, even if it does not reach the highest WHR efficiency, can provide the highest net power output with also a competitive investment cost per kW_e. The Authors though, did not show the analysis procedure and did not considered the adoption of pre-compression, which can increase the net power output of the cycle without an excessive increment of the plant complexity and investment costs. In addition, the techno-economic study considered high capacity sCO_2 systems, with a power scale ranging from 5 MW_e up to 10 MW_e.

Further configurations have been proposed also by other Authors for different uses. In particular, Binotti et al. [49] investigated three different sCO_2 power cycles for solar applications: the re-compression with and without the intercooling on the main compression and the partial cooling architectures. Park et al. [50] instead, studied three additional and more complex cycle layouts powered by a 1440 MW coal fired burner. The results showed that the highest performances were achieved in the case of single compression, a split regeneration and a triple expansion of the working fluid (thermal efficiency of 43.9% and a net power production of 634 MW_e). The Authors also found that adopting a transcritical CO_2 power unit to recover the heat rejected by the sCO_2 Brayton cycle gas cooler could lead to an improvement of the thermal efficiency between 1.5% and 2.3%. Other Authors considered the adoption of a bottoming unit to the sCO_2 Brayton power cycle to recover the large amount of heat rejected by the gas cooler. Song et al. [51] referred to a simple regenerated and a re-compression cycles for geothermal and WHR applications equipped with an ORC bottoming power unit. They also evaluated the impact of the adoption of a pre-cooler on the system performance. Concluding that the simple regenerated layout with the pre-cooler can achieve the highest thermal efficiency, namely up to 19%. Mohammad et al. [52] eventually performed a thermodynamic analysis of a re-compression sCO_2 system coupled with a bottoming Kalina cycle concluding that this configuration allows to increase

the overall thermal efficiency up to 10%, with respect to the re-compression standalone unit.

The power scale of sCO_2 systems analysed so far in literature is not suitable for high temperature stationary WHR applications which could provide power outputs in the order of tens or hundreds of kilowatts due to the widespread nature of the waste heat sources. Nonetheless, these streams have a remarkable impact on overall consumptions reduction since they are responsible of a global energy waste of 4.79 PWh/year [2]. Suitable systems to tackle the aforementioned opportunities should be small-scale plug and play sCO_2 power units whose technical and economic viabilities have not been addressed yet. In fact, the TRL of small scale sCO_2 systems has been estimated to be at the third level out of nine [53].

The current research work aims at filling this gap of knowledge and presents a holistic assessment of the theoretical capabilities of eight different sCO_2 cycle layouts for small-scale high-grade heat to power conversion applications. Unlike nuclear or solar power contexts, the nature of the heat source involves different goals and constraints such as reduced heat transfer coefficient, need to decrease pressure losses in the CO_2 heater and increased maintenance requirements to avoid excessive fouling when dirty exhausts are employed as heat source. The analysis further includes an estimation of the investment costs of heat exchangers and turbomachinery with reference to literature correlations, which were further validated through actual budgetary quotations requested by the Authors during the design of a 50 kW_e sCO_2 power unit. The design configurations are compared with reference to the same turbine inlet temperature and in terms of performances, exergy losses and several economic indicators, such as the Specific Cost per unit power (SC), the Internal Rate of Return (IRR), the Levelized Cost Of Electricity (LCOE) and the Payback Period (PBP). Among these architectures, an innovative layout which combines the features of the pre-compression and the pre-heating configurations is presented, and compared with the literature ones. The results show that even if this innovative cycle can achieve high performance with limited additional investment cost, the simple regenerated layout still maintains the highest economic convenience.

2. Cycle layouts

In this study eight different Brayton cycle layouts have been investigated to assess the best performing configuration with particular reference to WHR applications. All the architectures and the corresponding entropy diagrams are reported in Figs. 1 and 2.

The most essential layout is the Simple Regenerated one (SR – Fig. 1a), where the CO_2 is compressed near the critical point and then heated through a regenerative heat exchanger named recuperator. The actual heat recovery from the heat source takes place in a second heat exchanger commonly referred to as heater. Afterwards, the high enthalpy CO_2 is expanded in the turbine and later cooled in the low-pressure side of the recuperator. Before being compressed once again in the next cycle, the working fluid at the recuperator outlet is further cooled in a third heat exchanger called cooler, in which the actual heat rejection to the heat sink takes place. The excess of expansion power that is not used to drive the compressor and to overcome mechanical losses, is eventually converted in an electrical form through a generator.

With respect to the SR layout, the Re-Heating (RH – Fig. 1b) and the Re-Compression (RC – Fig. 1c) ones differ for a split expansion and a split compression respectively. In the re-heating cycle, the working fluid downstream the first turbine is heated up again in a secondary heater and undergoes to a second expansion; this results in a greater expansion work for the same power input required for compression and, in turn, to a greater overall efficiency and net power output. In the re-compression configuration, the sCO_2 stream is split downstream the low-pressure side of the low temperature recuperator. The main flow is then cooled in the gas cooler and eventually compressed by the main compressor, while the split flow is directly compressed and joins the main flow at the outlet of the high-pressure side of the low temperature recuperator. The split compression is adopted to have a better matching of the temperature profiles in the gas cooler and in the low temperature recuperator, and to decrease the amount of heat rejected by the working fluid into the environment. The Re-Compression Re-Heating layout (RCRH – Fig. 1d) eventually embeds both the aforementioned solutions to achieve even a higher cycle efficiency, and it is therefore characterized by a greater number of components and plant complexity.

Apart from these configurations, which have been typically developed for concentrated solar power and nuclear applications, additional layouts conceived for WHR purposes are also reported. The distinctive feature of these architectures is the maximization of the waste heat utilization of the hot source and, in turn, of the electrical net power output produced. Among them, the least complex cycle scheme is the Pre-Heating one (PH – Fig. 2a), in which the flow is split downstream the compressor and separately heated in the pre-heater and in the recuperator. Afterwards, the two contributions merge downstream these components, go to the primary heater and finally expand up to the lowest cycle pressure. This arrangement allows to have a better matching between the working fluid temperature glide and the hot source one such that a greater heat utilization is achieved.

With respect to the PH architecture, the Pre-Heating with Split Expansion (PHSE – Fig. 2b) and the Split-Heating with Split Expansion (SHSE – Fig. 2c) are characterized by greater complexity. In fact, in both cases the flow is split downstream the compressor, heated up separately in two parallel branches and eventually expanded in two turbines at different inlet temperatures. On the other hand, a less complex layout that the Authors propose is the Pre-Heating with Pre-Compression (PHPC – Fig. 2d), which respect to the PH architecture embeds only an additional compressor and a gas cooler. A summary of the equipment involved in each layout is given in Table 1.

3. Methodology

The different cycle configurations were investigated from both thermodynamic and economic perspectives. In particular, 1st and 2nd laws steady state analyses were carried out using the software CycleTempo™ [54] coupled with the NIST thermophysical property database [55]. To set up the sensitivity analysis, which allowed to identify the operating parameter that mostly affects the sCO_2 cycle performance, and to perform parametric studies at different operating ranges, the two software were further linked with a MATLAB® script. Finally, the economic assessment was performed with reference to literature correlations as well as budgetary quotations that the Authors requested during their ongoing design of a small-scale simple regenerated sCO_2 test rig at Brunel University London.

3.1. Energy analysis

The governing equations for cycle analysis are the steady state mass and energy balances. In particular, for each component of the system, heat exchanger or split/joint location Equations (1)–(3) respectively apply:

$$\dot{m}_i = \dot{m}_o \tag{1}$$

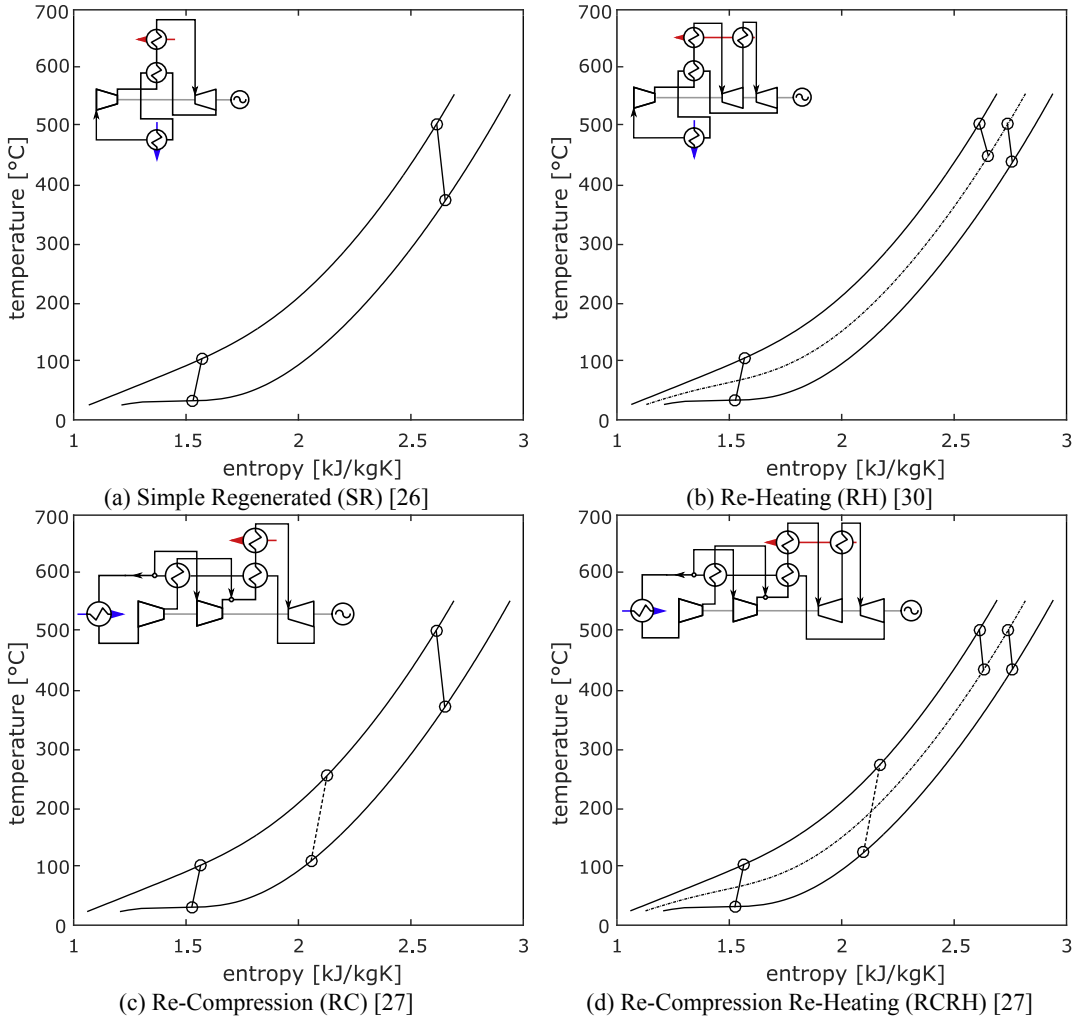

Fig. 1. sCO_2 cycle architectures proposed for nuclear and solar power applications.

$$\dot{m}_{hs}(h_i - h_o)_{hs} = \dot{m}_{cs}(h_o - h_i)_{cs} \tag{2}$$

$$\sum_{j=1}^{IN} \dot{m}_{i,j} h_{i,j} = \sum_{j=1}^{OUT} \dot{m}_{o,j} h_{o,j} \tag{3}$$

where *IN* and *OUT* are respectively the total number of flows merging and splitting from the *j*-th node considered.

As concerns the turbomachines, isentropic efficiency, inlet temperature and pressures at the inlet and outlet of the machine are the input data. Hence, enthalpy at the turbine and compressor outlets are computed through Equations (4) and (5) respectively, while for the temperature at the machine outlets Equation (6) applies.

$$h_{T,o} = h(p_o, s_i)\eta_{T,is} \tag{4}$$

$$h_{C,o} = h(p_o, s_i) \Big/ \eta_{C,is} \tag{5}$$

$$T_o = T(p_o, h_o) \tag{6}$$

Electrical power produced by the turbines or required by the compressors are calculated using Equations (7) and (8). The parameters η_m and η_e, whose values are reported in Table 2, refer to the mechanical and electrical efficiencies.

$$\dot{W}_T = \dot{m}_T (h_{T,i} - h_{T,o}) \eta_m \eta_e \tag{7}$$

$$\dot{W}_C = \dot{m}_C (h_{C,o} - h_{C,i}) / (\eta_m \eta_e) \tag{8}$$

Net power output and overall efficiency of the cycle are eventually calculated as per Equations (9) and (10):

$$\dot{W}_{net} = \sum_{j=1}^{NT} \dot{W}_{T,j} - \sum_{j=1}^{NC} \dot{W}_{C,j} \tag{9}$$

$$\eta_{tot} = \frac{\dot{W}_{net}}{\dot{m}_{hot}(h_{hot,i} - h_{hot,o})} \tag{10}$$

where *NT* and *NC* are respectively the number of turbines and compressors installed in each layout, as shown in Table 1.

3.2. Exergy analysis

Assuming that the dead state is defined at ambient conditions (1 bar, 25 °C), inlet and outlet exergy flows for each sCO_2 stream in each component are calculated as per Equations (11) and (12):

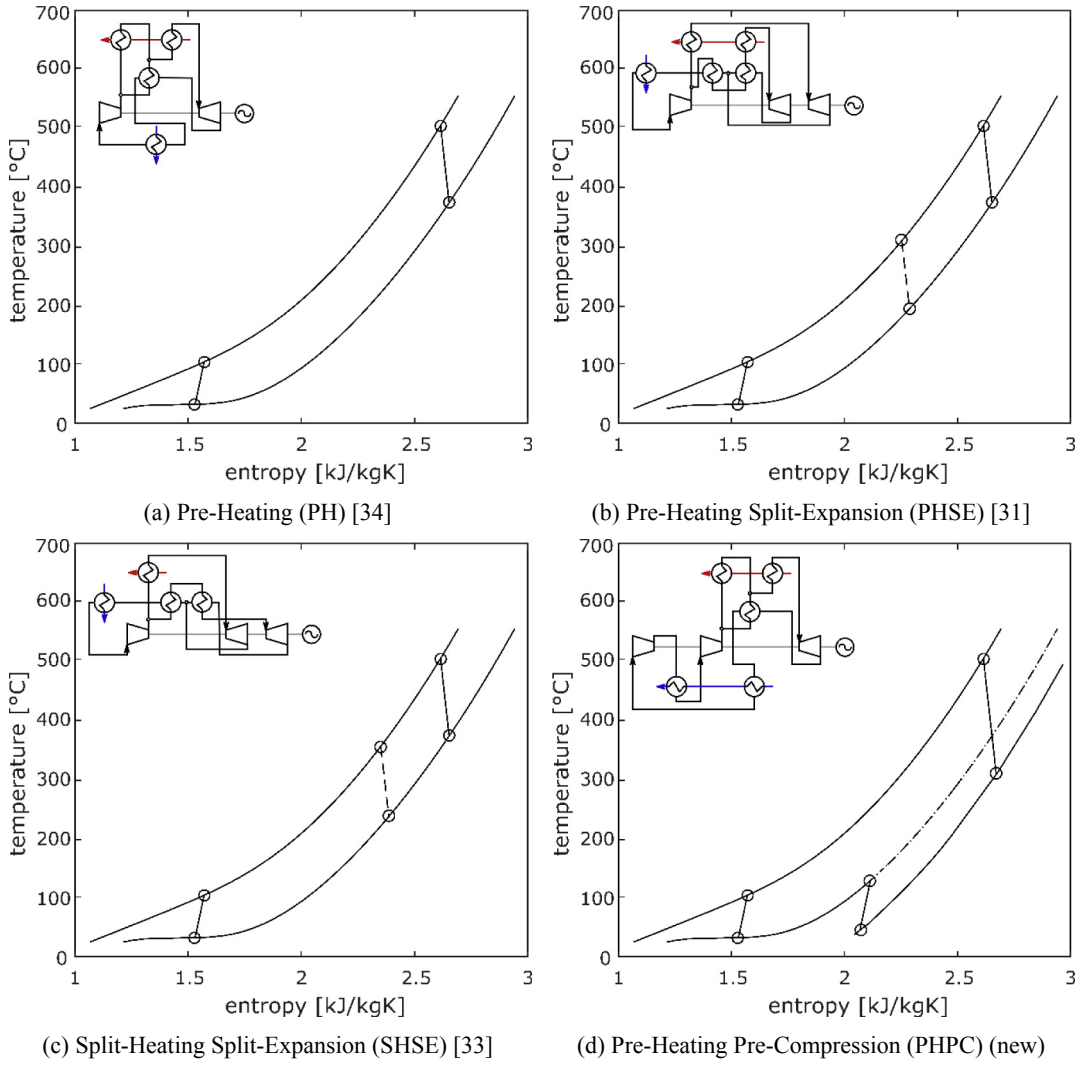

(a) Pre-Heating (PH) [34]

(b) Pre-Heating Split-Expansion (PHSE) [31]

(c) Split-Heating Split-Expansion (SHSE) [33]

(d) Pre-Heating Pre-Compression (PHPC) (new)

Fig. 2. sCO_2 cycle architectures for waste heat to power conversion.

Table 1
Equipment summary for the cycle layouts displayed in Figs. 1 and 2.

	SR	RH	RC	RCRH	PH	PHSE	SHSE	PHPC
Compressors (*NC*)	1	1	2	2	1	1	1	2
Turbines (*NT*)	1	2	1	2	1	2	2	1
Heaters	1	2	1	2	2	2	1	2
Recuperators	1	1	2	2	1	2	2	1
Coolers	1	1	1	1	1	1	1	2
Total heat exchangers (*NHX*)	3	4	4	5	4	5	4	5
Total turbomachines	2	3	3	4	2	3	3	3
Total components	5	7	7	9	6	8	7	8

$$\dot{E}_i = \dot{m}_i(h_i - T_0 s_i) \tag{11}$$

$$\dot{E}_o = \dot{m}_o(h_o - T_0 s_o) \tag{12}$$

The exergy irreversibility for heat exchangers can be evaluated through Equation (13), while Equation (14) applies for the compressors and Equation (15) for the turbines.

$$\dot{I}_{HX} = \dot{E}_{cs,i} + \dot{E}_{hs,i} - \dot{E}_{cs,o} - \dot{E}_{hs,o} \tag{13}$$

Table 2
Constant parameters in the sensitivity analysis.

Hot/Cold sources	Inlet temperature	Outlet temperature	Mass flow rate
Hot source – flue gas	650°C	350°C	1 kg/s
Cold source – water	15°C	45°C	not fixed
Turbomachines	Compressor		Turbine
Isentropic efficiency	0.70 [58]		0.85 [19]
Mechanical eff. (η_m)		0.95	
Electrical eff. (η_e)	0.91		

$$\dot{I}_C = \dot{E}_{C,i} + \dot{W}_C - \dot{E}_{C,o} \tag{14}$$

$$\dot{I}_T = \dot{E}_{T,i} - \dot{W}_T - \dot{E}_{T,o} \tag{15}$$

Therefore, the overall exergy efficiency of each thermodynamic cycle can be calculated through Equation (16):

$$\eta_{ex} = 1 - \frac{\sum_{j=1}^{NC} \dot{I}_{C,j} + \sum_{j=1}^{NT} \dot{I}_{T,j} + \sum_{j=1}^{NHX} \dot{I}_{HX,j} + \dot{E}_{hot,o}}{\dot{E}_{hot,i}} \tag{16}$$

where the $\dot{E}_{hot,o}$ is the exergy flow of the exhaust gases downstream the primary heater (Equation (12)).

3.3. Economic indicators

In order to assess economic aspects of the different layouts analyzed, several economic indicators have been considered, namely the Specific Cost (SC), the Levelized Cost Of Electricity (LCOE), the Internal Rate of Return (IRR) and the Payback Period (PBP).

The SC is a simple indicator representing the unitary cost of a plant per electrical kilowatt (kW_e) installed and can give a qualitative idea to compare similar systems.

$$SC = \frac{C_{tot}}{\dot{W}_{net}} \tag{17}$$

In Equation (17), the numerator is the investment cost of the sCO_2 system that not only accounts for the cost of the equipment but also for the ancillaries as well as the installation costs (Equation (18)).

$$C_{tot} = \left(\sum_{j=1}^{NHX} C_{HX,j} + \sum_{j=1}^{NT} C_{T,j} + \sum_{j=1}^{NC} C_{C,j} \right) C_{inst} \tag{18}$$

The investment cost of the heat exchangers was calculated using the data available in Ref. [56]. These correlations refer to a specific cost per heat transfer capacity (UA-value), which in turn depends on the heat exchanger duty and the Logarithmic Mean Temperature Difference (LMTD), as shown in Equation (19). Therefore, this approach allows an estimation of the costs without going into a detailed exchanger modelling. Nevertheless, the costs calculated with Equation (19) are in well agreement with budgetary quotations requested to multiple manufacturers of sCO_2 heat exchangers. Values for the λ coefficient, which depends on the type of heat exchanger considered and its technology (heater, recuperator or cooler), are reported in Table 5.

$$C_{HX,j} = \lambda (UA)_j = \frac{\lambda Q_j}{LMTD_j} \tag{19}$$

Costs for turbine and compressor can be calculated according to Equations (20) and (21). These correlations relate the investment cost to operating parameters of the machines, such as mass flow rates, pressure ratio, isentropic efficiency and turbine inlet temperature expressed in Celsius degrees [57].

$$C_T = 479.34\, \dot{m}_T \left(\frac{1}{0.93 - \eta_T} \right) \ln(\beta_T) \left(1 + \exp(0.036\, T_{T,i} - 54.4)\right) \tag{20}$$

$$C_C = 71.10 \dot{m}_C \left(\frac{1}{0.92 - \eta_C} \right) \beta_C \ln(\beta_C) \tag{21}$$

The plant installation costs were taken into account through a multiplier of the investment cost equal to 30%. This coefficient is slightly overestimated to also include the cost for the auxiliaries (i.e. refrigeration compressors for drainage removal, motorized valves, electrical connections etc.).

Unlike SC, the LCOE is instead a more general metric that allows to assess the profitability of an investment in a generic power plant. In fact, the LCOE estimates the average cost of the electricity that will be produced by the facility. This parameter can be calculated according to Equation (22) as the ratio of the Present Value of the plant Expenses (PVE) and the plant productivity over its total operating time, which in turn depends from the net electrical power, the lifetime and the utilization factor. These parameters are all reported in Table 5.

$$LCOE = \frac{PVE}{8760\ u\ NY\ \dot{W}_{net}} \tag{22}$$

The PVE, whose formulation is reported in Equation (23), involves the cash flows calculation of the plant expenses through Equation (24). In this study, operation and maintenance costs per kW_e of power installed are taken into account through the parameter *OM* while the escalation rate of this cost over the years is considered through the coefficient *er*. These information are reported in Table 5 together with the discount rate *r*.

$$PVE = C_{tot} + \sum_{k=1}^{NY} \frac{CF_{xp,k}}{(1+r)^k} \tag{23}$$

$$CF_{xp,k} = \dot{W}_{net} \left(OM(1+er)^k \right) \tag{24}$$

The IRR is a financial metric indicating the final value of the investment interest rate to get a Net Present Value (NPV) equal to zero with reference to the plant lifetime as interval period. According to this definition, the IRR was calculated as per Equation (25). In this case, the cash flows of the plant revenues must be also considered; the reference formulation is reported in Equation (26) where C_e is the cost of electricity, whose value is presented in Table 5 and decreased over the plant lifetime through the coefficient *dr*.

$$-C_{tot} + \sum_{k=1}^{NY} \frac{CF_{rev,k} - CF_{xp,k}}{(1+IRR)^k} = 0 \tag{25}$$

$$CF_{rev,k} = \dot{W}_{net} \left(8760u\ C_e (1-dr)^k \right) \tag{26}$$

Finally, the PBP represents the time required to recover the initial investment for each plant layout. Because of the degradation of the productivity and the increase of the maintenance costs, the revenues are uneven during the system operating lifetime, so the cumulative cash flows for all the layouts are computed for each year of the operating lifetime. Then, the approximated PBP is the year (Y_A) when this cumulative cash flow (CF_{cum,Y_A}) becomes positive. However, to get a more accurate figure, the Equation (27) is used, where CF_{rev,Y_A} and CF_{xp,Y_A} indicate the revenues and the expenses for that specific period.

$$PBP = Y_A - \frac{CF_{cum,Y_A}}{CF_{rev,Y_A} - CF_{xp,Y_A}} \quad (27)$$

3.4. Solution routine

A general flow chart of the calculation procedure is shown in Fig. 3 and applies to all the architectures investigated. Each cycle layout is preliminary built in the Cycle Tempo™ environment by assembling a series of standardized components considered as black boxes and characterized by their distinctive features: turbines and compressors by the isentropic efficiencies, pressure ratio, and inlet temperature; heat exchangers by the pinch point.

Based on the number of mass and energy equations that can be written for a given cycle layout, a system of linear equations is built and solved iteratively. The coefficient matrix of the system contains also the enthalpies computed in the previous iterations while the vector of unknowns is populated with the mass flow rates in each pipe of the physical system, whose number is equal to the one of the components. The vector of constants eventually contains thermal or electrical powers provided as inputs. During the iterative procedure, enthalpy calculation occurs through a Dynamic-Link Library (DLL) to the NIST database [55]. Once the mass convergence criterion is satisfied, energy and exergy performance parameters are calculated.

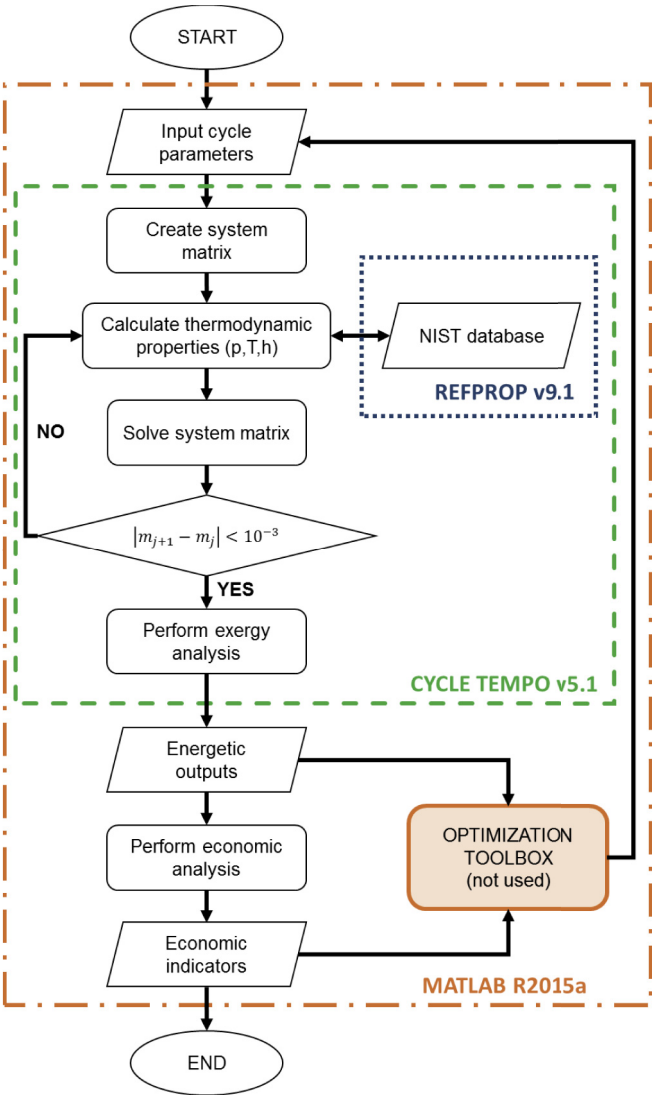

Fig. 3. Flow chart of the solution routine.

The difference in the resolution of simple or complex cycle layouts lies in the size of the matrixes but not in their structure. An additional element of complexity can be due to specifying pressure and heat losses in the pipes or heat exchangers since this would make the coefficient matrix more dense. In the current study, however, these details were discarded to make the comparison more consistent.

Fluid property variation inside the heat exchangers is instead taken into account during the creation of temperature-enthalpy diagrams for each device in order to check that the crossing of the temperature profiles is prevented. In order to do that, a discretization based on the share of thermal power exchanged is carried out and allows to trace the heat transfer curves.

To automate the calculations for parametric and optimization studies, Cycle Tempo™ has herein run in batch mode through a script developed in the Matlab® environment which also included the economic correlations of paragraph 3.3. A further advantage of this approach is the possibility to use the Matlab® Optimization toolbox. This feature is particularly handy in the design of a specific cycle for a given application. With regards to the goal of the current study, however, a comparison between optimized configurations would have been inconsistent since the cycle parameters would have differed from a layout to another one. Hence, the optimization feature was not employed.

4. Sensitivity analysis

In general terms, the sCO_2 power cycle performance are affected by several thermodynamic parameters such as: pressure ratio, operating conditions at the compressor inlet, turbine inlet temperature, pressure losses inside the system, turbomachinery efficiency, hot source inlet temperature and mass flow rate, and pinch point in the heat exchangers. Therefore, a comprehensive techno-economic comparison between different plant layouts should accurately consider the different design conditions and operating modes. However, such a comparison would not only imply high computational and post-processing efforts but could also be inconsistent. As a consequence, a sensitivity analysis was carried out beforehand to understand the thermodynamic parameter that mostly affected the plant performance, such that the different operating regimes in the techno-economic analysis could be expressed in terms of this variable.

To perform this preliminary analysis, several simulations have been carried out using as reference layout the simple regenerated one. The influence of the cycle operating parameters has been compared in terms of net electrical power output due to the relevance of this quantity in waste heat recovery applications. The dependent variables investigated are temperature (TIC) and pressure (PIC) at the compressor inlet, the turbine inlet temperature (TIT), the pinch point of the heat exchangers (PP_{HX}) and the maximum cycle pressure (POC). On the other hand, the inlet and outlet conditions of the hot and the cold sources have been kept constant together with their respective mass flow rates. Similarly, the isentropic efficiencies of the turbomachines were assumed as constant and equal to the values measured at Sandia National Laboratories during the testing campaign on the 300 kW re-compressed sCO_2 power cycle test rig unit [19,58]. In particular, the compressor efficiency was taken from Ref. [58], in which a compressor having the same power size of the one considered in the current study was tested at different operating conditions. The experimental campaign showed that, in the whole range of

pressure and temperatures considered in our analysis, an efficiency of 0.7 was always achievable acting on the compressor speed. For the turbine efficiency, in Ref. [19], a sCO_2 turbine was tested for a pressure ratio of 1.24, a mass flow rate of 1.74 kg/s, and an inlet temperature of 391 °C and reached an efficiency of 0.846. Since in our case we took in account a pressure ratio of 2.63 and a slightly higher range of mass flow rates, the assumed efficiency of 0.85 can be considered a conservative choice. In fact, turbine isentropic efficiency generally increases with pressure ratio, inlet temperature and mass flow rate of the working fluid. Finally, the values considered for mechanical and electrical efficiencies come from design considerations that the supplier of the electrical generator for the sCO_2 system under construction at Brunel University shared with the Authors. Table 2 summarizes the constant parameters considered in the sensitivity analysis while Table 3 reports the variation of the independent variables with respect to a reference case, which is an intermediate point within the operating range considered in this work that is suitable for sCO_2 applications and generates a power output of 100 kW_e.

In Fig. 4, the results of the analysis are reported. The variation of the net power output produced by the SR configuration is displayed, both in relative and absolute terms, as a function of the several input parameters. For each set of simulation, one variable has been decreased or increased while the others were maintained constant and equal to the values in the reference case. Among all these variables, the ones that least affect the plant power output are the minimum and the maximum pressures of the cycle, and the pinch point in the heat exchangers. In fact, considering a change of the compressor inlet pressure from 74 bar to 80 bar, the net power output increases only from 96 kW to 101 kW. The same small variations can be observed for the compressor outlet pressure and for the heat exchangers' pinch points; in fact, the net power output changes from 93 kW to 100 kW when the maximum pressure is set respectively from 150 bar to 220 bar, and from 101 kW to 95 kW when the pinch points are set respectively from 10 °C to 20 °C.

More pronounced is instead the effect of the compressor inlet temperature, since the net power output of the system decreases from 104 kW to 93 kW due to a greater compressor input power when TIC increases from 32 °C to 38 °C. This analysis also shows that the worsening of the overall system performance when the compression of the working fluid occurs far from the critical point is primarily due to the temperature rather than a pressure increase, in agreement with the literature.

Nonetheless, the most influencing parameter for the sCO_2 performance is undoubtedly the turbine inlet temperature (TIT). In fact, when this variable increases from 350 °C to 550 °C, the plant power output variation is maximized, going from 74 kW to 115 kW. For this reason, the turbine inlet temperature has been chosen as dependent variable for the techno-economic cycle comparison reported in Section 5.

5. Results and discussion

Due to the diversity that characterizes the sCO_2 cycle layouts considered in Section 2, to perform a consistent performance comparison, a given number of assumptions had to be made. First of all, the analysis is carried out with reference to 1.0 kg/s of flue gas at 650 °C, such that all the results could be easily scaled for any high temperature heat source, provided that the gas composition leads to the same specific heat at constant pressure (1.1 kJ/kgK). As concerns the final temperature of the hot source after the heat recovery, two main approaches are pursued: the cycle layouts similar to the SR one (i.e. RC, RH and RCRH), in which the sCO_2 flow is not split in two branches, considered a outlet gas temperature of 350 °C, as it was assumed in the sensitivity analysis reported in Section 4. On the other hand, for the cycle schemes more oriented to WHR applications such as the PH, PHPC, SHSE and PHSE ones, the outlet gas temperature has been set equal to 150 °C, which is the conventional threshold to prevent low temperature corrosion issues. Therefore, this second category of layouts is characterized by high recovery potential compared to the first set of cycle schemes. In fact, without a flow split, an outlet temperature of 150 °C cannot be achieved in the first family of cycle architectures since the temperature profiles of flue gas and CO_2 in the heater would intersect. Conversely, splitting the sCO_2 stream allows a suitable matching with the temperature glide of the heat source and, in turn, to maximize the heat utilization.

On the other hand, those simulation parameters that apply only to a subset of cycle architectures have been optimized for each simulation in order to achieve the maximum net power output and thus compare only optimal layouts. Example of such variables are

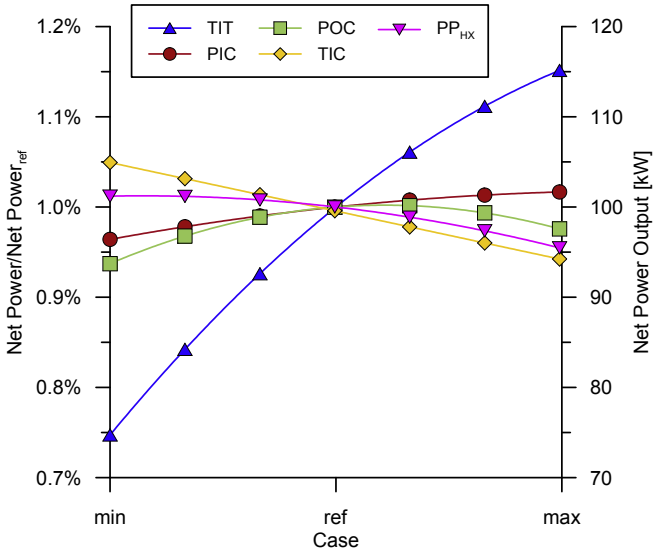

Fig. 4. Sensitivity analysis on the net power output and with reference to the SR layout (Fig. 1a).

Table 3
Ranges of variation for the independent variables of the sensitivity analysis.

	min	ref	max
PIC [bar]	74	76	80
TIC [°C]	32	35	38
POC [bar]	150	200	250
TIT [°C]	350	450	550
PP_{HX} [°C]	10	15	20

Table 4
Assumptions in the thermodynamic comparison (NA = not applicable, OPT = optimized).

	SR	RH	RC	RCRH	PH	PHSE	SHSE	PHPC
Water T_i [°C]	15							
Water T_o [°C]	45							
Water $\dot{m}$ [kg/s]	not fixed							
Compressor p_i [bar]	74							
Compressor p_o [bar]	200							
Flue gas $\dot{m}$ [kg/s]	1							
Flue gas T_i [°C]	650							
Flue gas T_o [°C]	350	350	350	350	150	150	150	150
Split ratio	NA	NA	OPT	OPT	OPT	OPT	OPT	OPT
Pre-compressor p_i [bar]	NA	NA	NA	NA	NA	NA	NA	60

the split ratio for the RC layout or the pre-compressor inlet pressure for the PHPC configuration. Finally, the efficiencies assumed for the turbomachines are reported in Table 2, while Table 4 summarizes the values of the parameters kept constant throughout the study. Among them, it is assumed that the cold source is a water stream whose mass flow rates varies such that an inlet temperature at the cooler of 15 °C and an outlet temperature of 45 °C are always maintained.

5.1. Thermodynamic analysis

Figs. 5 and 6 show the net power output and the overall energy efficiency in each layout at turbine inlet temperatures from 250 °C to 600 °C. However, not all the configurations analyzed can operate in the range considered since, at high TIT, some schemes might present an intersection of the temperature profiles of the flue gases and the CO_2 in the heater. These cases have not physical meaning and they have been therefore omitted from the results. For instance, the maximum TIT displayed for the PHPC architecture is equal to 475 °C, since it is the highest value achievable by the architecture.

Considering then only the meaningful cases, both the figures show the positive effect that an increase of the TIT has on the cycle performance. Among the more conventional sCO_2 layouts, Fig. 5 shows that the ones which generate a higher power output are the RH and the RCRH ones, thanks to the split expansion feature. Indeed, when the TIT goes from 250 °C to 400 °C these two configurations generate from 59 kW to 95 kW and from 49 kW to 98 kW of electric power respectively, against the one produced by the SR and the RC configurations that in the same range of temperature goes from 51 kW to 89 kW and from 38 kW to 90 kW respectively. Beyond 400 °C, in RH and RCRH layouts, the split of the heat load in two separate heaters limits the achievable TIT. This fact, on one hand allows to enhance the cycle efficiency (Fig. 6) but on the other one it constraints the power output (Fig. 5). Therefore, in absolute terms, the SR and the RC layouts eventually show higher performance, since they allow to produce 115 kW and 113 kW of electric power at TIT of 550 °C and 500 °C respectively.

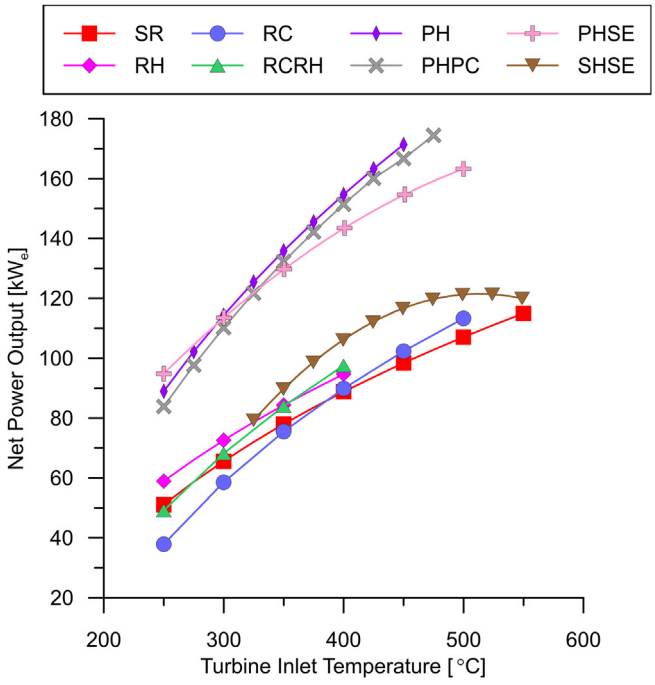

Fig. 5. Net power output comparison.

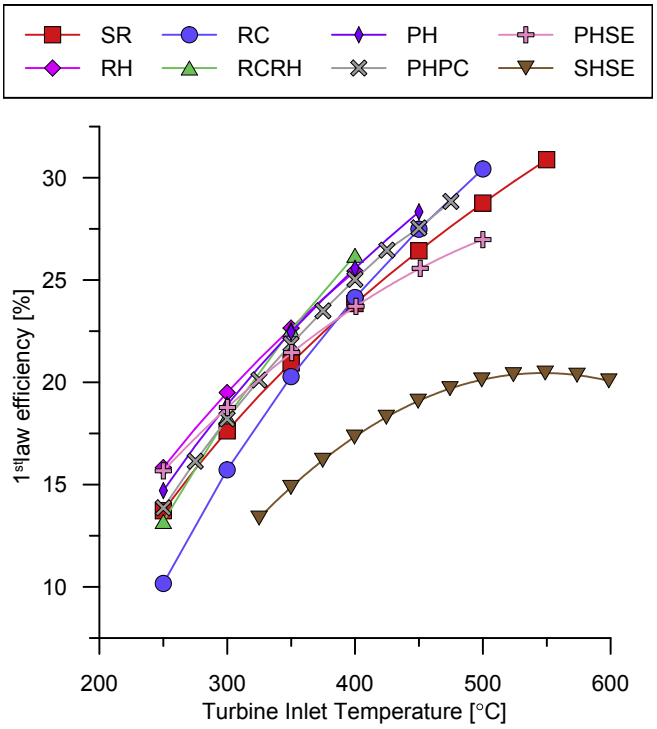

Fig. 6. 1st law (energy) efficiency comparison.

The layouts conceived for WHR applications are able to harvest a greater amount of thermal power from the heat source. To balance this higher thermal load, a greater amount of CO_2 is required in these systems. This results in power outputs higher than those that characterize the configurations previously mentioned but, on the other hand, also in lower overall efficiency since the relative increase of thermal power recovery (that appears in the denominator of Equation (10)) is greater than the relative increment in electrical power output. The SHSE layout, at 500 °C and 550 °C, is able to generate up to 119 kW and 121 kW of electric power, more than the one produced by the SR and RC configurations at the same TITs. A much higher net power output can be generated by the PHSE, PHPC and PH architectures that, with a maximum cycle temperature of 450 °C, are able to produce up to 153 kW, 167 kW and 171 kW respectively. In absolute terms however, the layout which shows the higher power output is the PHPC one which, thanks to the addition of a pre-compressor, allows to increase the expansion ratio across the turbine and thus to generate up to 174 kW with a TIT of 475 °C against the 171 kW of the PH configuration at a TIT of 450 °C.

Regarding the exergy efficiency, it is possible to see from Fig. 7 that all the layouts show, on average, similar performance. For low TIT, the RH configuration shows higher efficiencies, going from 15.8% up to 19.9% when the TIT goes from 250 °C to 350 °C. At a TIT of 400 °C the RCRH performs better, with an efficiency equal to 26.2%. At a TIT equal to 450 °C, the PH layout achieves a higher efficiency, namely 28.3%. The highest performances are however shown by the RC and the SR architectures, which present efficiency values of 30.9% and 30.4% at a TIT of 500 and 550 °C respectively.

Lower efficiencies are achieved by the SHSE configuration (20.4% at a TIT of 600 °C), since the sCO_2 flow, which is heated from the low and high temperature recuperators, expands at lower TIT. The lower net power output additionally affects the exergy efficiency of this layout, which in fact is the lowest among its similar architectures. The SHSE scheme presents indeed a maximum

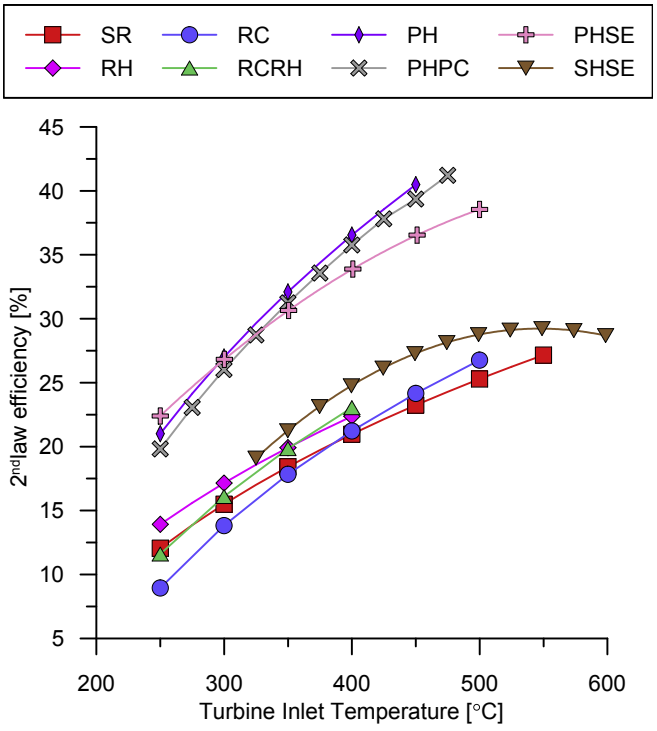

Fig. 7. 2nd law (exergy) efficiency comparison.

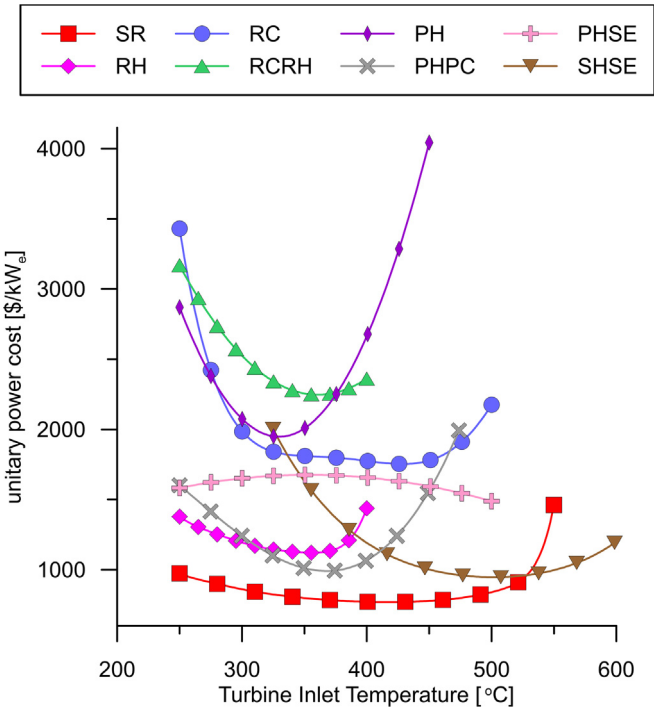

Fig. 8. SC comparison.

exergy efficiency of 29.3% against the 38.9%, 40.5% and the 41.2% of PHSE, PH and PHPC architectures (Fig. 7).

Worst exergy efficiencies are those achieved by the conventional sCO_2 cycle schemes since the outlet temperature of the heat source downstream the heat recovery process is still very high (350 °C). In fact, it is possible to notice that the SR and RC layouts show a maximum exergy efficiency respectively equal to 27.2% and 26.7% (for a TIT of 550 °C and 500 °C), while for the RH and the RCRH schemes, which are not able to reach that temperature, the maximum exergy efficiency achievable for a TIT of 400 °C is respectively equal to 22.4% and 26.2%.

5.2. Investment cost analysis

In each thermodynamic simulation, several financial metrics have been computed accordingly to formulations presented in the paragraph 3.3. Components cost data and additional parameters herein assumed are listed in Table 5. It is worth to notice that the specific cost for heat exchangers depends on the type and the technology, namely fin tube heater, printed circuit recuperator and plate heat exchangers as gas coolers. Although previous studies considered either printed circuit or shell and tube gas coolers, thanks to the increasing role of natural refrigerants in the refrigeration sector, plate heat exchangers are nowadays available also for CO_2 applications at low temperatures (<250 °C) but high pressure. Therefore, in the current analysis, the plate heat exchanger technology, which has a specific cost two orders of magnitude lower than the printed circuit one, was considered.

Table 5
Assumptions in the economic comparison.

Components	
λ Heater [$/UA]	5000
λ Recuperator [$/UA]	2500
λ Gas cooler [$/UA]	36
Plant	
O&M operations (*OM*) [$/kW$_e$]	30
O&M escalation rate (*er*) [%]	3
Plant degradation rate (*dr*) [%]	1
Electricity market price (C_e) [$/kWh]	0.06
Plant lifetime (*NY*) [years]	20
Plant utilization factor (*u*) [%]	85
Discount rate (*r*) [%]	5
Plant installation cost (C_{inst})	1.3

Figs. 8 and 9 show, the Specific Cost for kW$_e$ installed (SC) and the Levelized Cost Of Electricity (LCOE) for the eight layouts as a function of the TIT. The results obtained for both the indicators present the same tendency, since both of them can be seen as the ratio between total investment cost and power production capacity. In each layout, SC and LCOE show a parabolic trend with a minimum cost for a turbine inlet temperature in a range between 325 °C and 425 °C. The only exceptions are represented by the SHSE and the PHSE configurations, which present the minimum cost point shifted towards 500 °C. These minima are mainly due to the fact that the cost of the units is driven by the heat exchangers' one. In fact, while the costs for turbomachines, auxiliaries and installation are, on average, constant between the range of power sizes analyzed in this work, the heat exchangers ones experience a remarkable variation due to their heat transfer area, which in turn depends on the Logarithmic Mean Temperature Difference (LMTD). Therefore, at low TIT, the size of the heat exchangers, and thus the costs, is reduced since the LMTD is large. However, the power generated by the unit is low and in turn the SC and LCOE become relevant. At higher TIT, the heat exchangers cost increases, but not excessively since the LMTD is still large, and so does the power produced by the plant, causing then a decrease of the SC and LCOE. Increasing even more the TIT, although it allows to have a higher net power output, it also leads to a reduction of the LMTD in the heat exchangers and especially in the heater, with a consequential increase of the heat transfer area, the heat exchangers' cost and thus the cost indicators.

A further interesting result is that the SR configuration, which

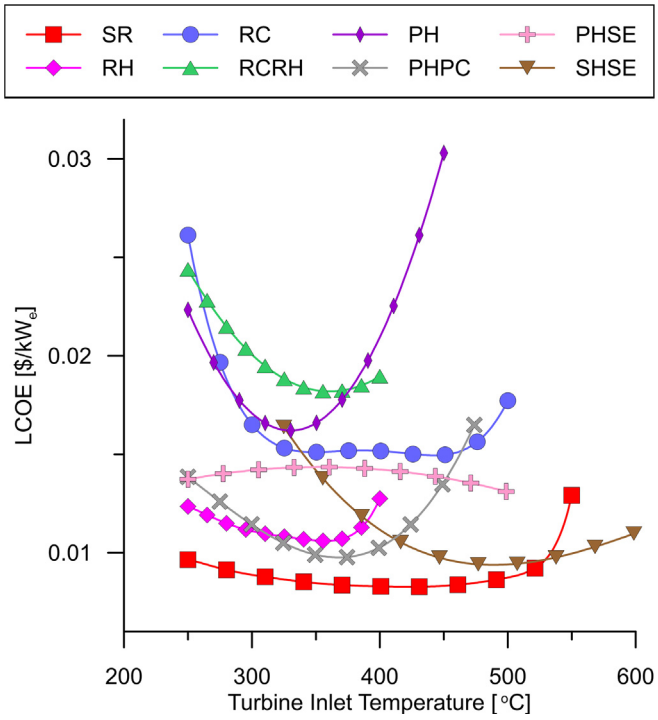

Fig. 9. LCOE comparison.

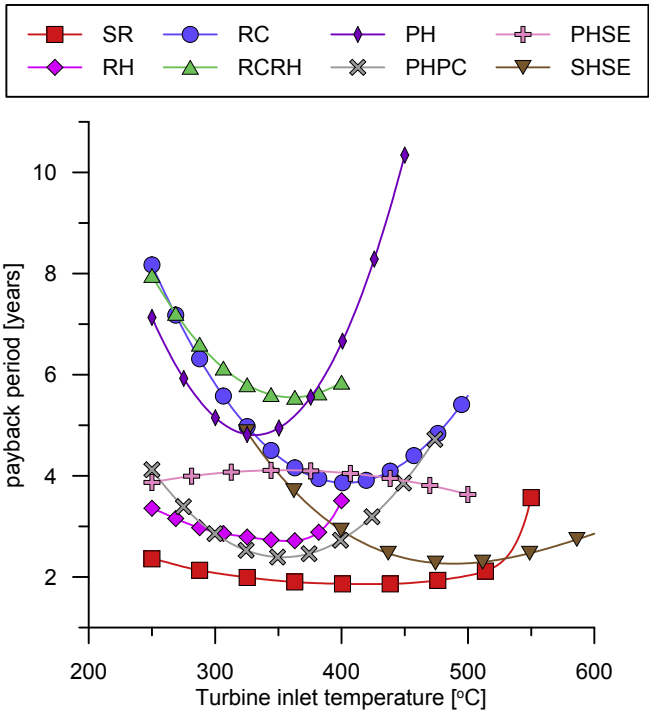

Fig. 10. PBP comparison.

has the lowest complexity and number of components, also presents the lowest minimum SC and LCOE, which are equal respectively to 770 $/kW$_e$ and 0.0083 $/kW$_e$ for a TIT of 425 °C. Even the architecture more oriented to WHR applications present higher SC and LCOE. Indeed, the PHSE and the PH configurations show a minimum SC, respectively at a TIT of 500 °C and 325 °C, equal to 1577 $/kW$_e$ and 1516 $/kW$_e$, and a minimum LCOE equal to 0.0137 $/kW$_e$ and 0.0130 $/kW$_e$; while the SHSE and PHPC show lower minimum specific costs, 981 $/kW$_e$ and 948 $/kW$_e$, and LCOE, 0.0095 $/kW$_e$ and 0.0097 $/kW$_e$, which however are still higher than the ones related to the SR architecture.

Among the conventional and more complex layouts, the RH scheme presents the minimum SC and LCOE, equal to 1123 $/kW$_e$ and 0.0106 $/kW$_e$ (at a TIT of 350 °C), which are also competitive with respect to the ones of the WHR plant schemes. Eventually, the RC and the RCRH architecture show much higher minimum costs, as 1775 $/kW$_e$ and 2247 $/kW$_e$ for the SC and 0.0150 $/kW$_e$ and 0.0182 $/kW$_e$ for the LCOE, respectively at a TIT of 400 °C and 350 °C.

The same considerations outlined above also hold for the payback period (Fig. 10), which shows the same trend lines of the two metrics before analyzed. In particular, it is possible to notice that the SR configuration presents a payback period of 1.86 years for a TIT of 425 °C, which is the lowest among all the layouts and it could be also attractive from a market perspective. Also the PHPC, the RH and the SHSE layouts present low payback periods, at a TIT of 325 °C, 350 °C and 500 °C, equal respectively to 2.38, 2.73 and 2.30 years, which are still interesting for heat to power conversion systems oriented to WHR industrial applications. One of the main reason for these promising outcomes is due to having considered a plate heat exchangers as gas coolers; indeed, this allows to drop the investment cost of nearly 20%.

Fig. 11 instead, shows the IRR again as a function of the TIT for all the eight different sCO_2 layouts. Also in this case the SR configuration shows the best IRR, equal to 53% for a TIT of 425 °C, while lower rates characterize the PHPC, RH and SHSE layouts, which show respectively a maximum IRR of 41%, 36% and 43% with a TIT of 325 °C, 350 °C and 500 °C. On the other hand, the PH configuration presents the worst rate, equal to 6% for a TIT of 450 °C. It is worth to notice that the results related to these two indicators, contrarily to the LCOE and SC parameters, are strongly affected by the electricity price chosen during the analysis (0.06 $/kWh), and the incentives and taxation rate assumed (which have been neglected in this work).

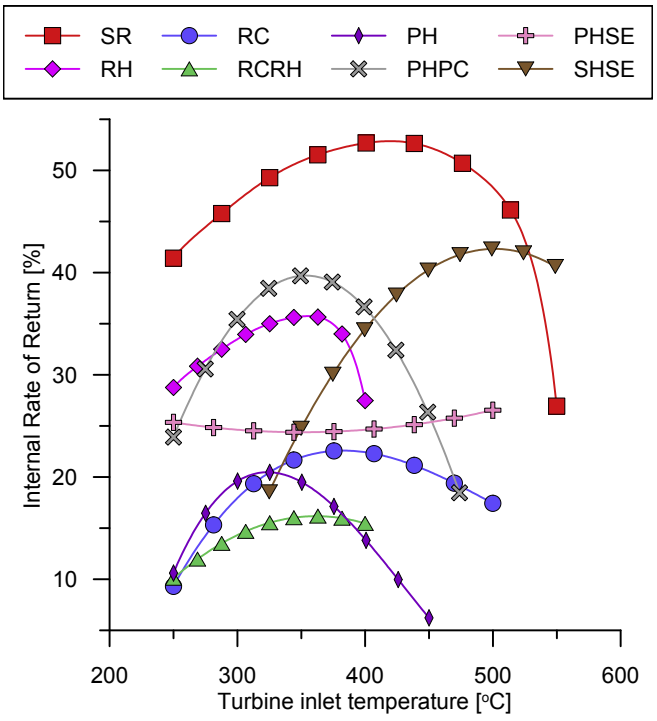

Fig. 11. IRR comparison.

6. Conclusions

This study presented a techno-economic analysis of eight different sCO_2 power cycle configurations. In particular, four layouts originally developed for concentrated solar power and nuclear applications, the simple regenerative (SR), RH, RC and RCRH, have been compared to architectures more oriented to waste heat recovery and conversion uses, such as the SHSE, PH, PHSE and PHPC. The net power output, the thermal and exergy efficiencies, and several investment cost parameters have been investigated at different plant operating conditions using cost correlations, and other published data and assumptions with particular reference to small to medium scale systems.

In order to address the most representative cycle variable to identify the variation of the system operating point, a sensitivity analysis has been carried out. The results showed that the turbine inlet temperature is the most influencing parameter on cycle net power output and overall energy and exergy efficiencies. The second most important parameter was identified to be the compressor inlet temperature, which must be very close to the critical point of the CO_2 working fluid.

The waste heat recovery and conversion architectures have been found to be able to generate a much higher net power output in comparison to the more conventional layouts, due to the higher amounts of waste heat they can recover. This results from the split-heating of the flow after the compression stage that also allows a better thermal matching between the CO_2 and hot source temperature profiles in the heater. Indeed, the SHSE, PHSE, PH and PHPC layouts have been found to produce 124 kW, 165 kW, 171 kW and 174 kW respectively, compared to 95 kW, 98 kW, 113 kW and 115 kW that would be generated by the RH, RCRH, RC and SR configurations respectively.

The novel PHPC architecture was found to be able to achieve the highest net power output. Nonetheless, the investment cost analysis revealed that the SR plant scheme, which is characterized by the lowest complexity, provides the highest economic effectiveness with a specific cost of 770 $/kW$_e$ and payback period of 1.86 years.

Even though the net power output and thermal and exergy efficiencies of the different cycle layouts were found to increase proportionally with the turbine inlet temperature (TIT), the investment cost parameters showed a parabolic variation, with maximum IRR in the range between 325 °C and 500 °C depending on the system architecture. This is due to the high contribution of the high temperature heat exchanger(s) to the overall cost of the system which increases with the exhaust gas temperature. Heater cost reduction is therefore very important to lower the overall capital cost of the sCO_2 power system and to increase its economic competitiveness.

Acknowledgement

The research presented in this paper has received funding from the European Union's Horizon 2020 research and innovation program under grant agreement No. 680599. Aspects of the work are also funded by the Centre for Sustainable Energy Use in Food Chains (CSEF). CSEF is an End Use Energy Demand Centre funded by the Research Councils UK, Grant No: EP/K011820/1. The manuscript reports all the relevant data to support the understanding of the results. More detailed information and data, if required, can be obtained by contacting the corresponding author of the paper.

References

[1] Cullen JM, Allwood JM. Theoretical efficiency limits for energy conversion devices. Energy 2010;35:2059–2069. doi:https://doi.org.10.1016/J.ENERGY.2010.01.024.
[2] Forman C, Muritala IK, Pardemann R, Meyer B. Estimating the global waste heat potential. Renew Sustain Energy Rev 2016;57:1568–1579. doi:https://doi.org.10.1016/J.RSER.2015.12.192.
[3] Hung T-C. Waste heat recovery of organic Rankine cycle using dry fluids. Energy Convers Manag 2001;42:539–53. https://doi.org/10.1016/S0196-8904(00)00081-9.
[4] Iglesias Garcia S, Ferreiro Garcia R, Carbia Carril J, Iglesias Garcia D. A review of thermodynamic cycles used in low temperature recovery systems over the last two years. Renew Sustain Energy Rev 2018;81:760–7. https://doi.org/10.1016/j.rser.2017.08.049.
[5] Tchanche BF, Lambrinos G, Frangoudakis A, Papadakis G. 2011-Tchanche - low-grade heat conversion into power using organic Rankine cycles A review of various applications. Renew Sustain Energy Rev 2011;15:3963–79. https://doi.org/10.1016/j.rser.2011.07.024.
[6] Wright SA, Pickard PS, Fuller R, Radel RF, Vernon ME. Supercritical CO_2 Brayton cycle power generation development program and initial test results. In: ASME 2009 Power Conf. ASME; 2009. p. 573–83. https://doi.org/10.1115/POWER2009-81081.
[7] Freund P, Bachu S, Simbeck D, Thambimuthu K, Annex I. Properties of CO2 and carbon-based fuels. IPCC Spec Rep. 2005.
[8] Persichilli M, Kacludis A, Zdankiewicz E. Supercritical CO_2 power cycle developments and commercialization: why sCO_2 can displace. Steam Ste. Power-Gen India; 2012.
[9] Huck P, Freund S, Lehar M, Peter M. Performance comparison of supercritical CO_2 versus steam bottoming cycles for gas turbine combined cycle applications.
[10] Parks C. Corrosion of candidate high temperature alloys in supercritical carbon dioxide. 2013.
[11] Sarkar J. Second law analysis of supercritical CO_2 recompression Brayton cycle. Energy 2009;34:1172–8. https://doi.org/10.1016/J.ENERGY.2009.04.030.
[12] Johnson G, McDowell M. Issues associated with coupling supercritical CO_2 power cycles to nuclear, solar and fossil fuel heat sources. In: Proc supercrit CO_2 power cycle; 2009.
[13] Weiland NT, White CW. Techno-economic analysis of an integrated gasification direct-fired supercritical CO $_2$ power cycle. Fuel 2018;212:613–25. https://doi.org/10.1016/j.fuel.2017.10.022.
[14] Ahn Y, Bae S, Kim M, Cho S, Baik S, Lee J. Cycle layout studies of S-CO_2 cycle for the next generation nuclear system application. Trans 2014:1–5. http://koasas.kaist.ac.kr/bitstream/10203/211352/1/ver4.0.pdf.
[15] Vitale Di Maio D, Boccitto A, Caruso G. Supercritical carbon dioxide applications for energy conversion systems. Energy Procedia 2015;82:819–24. https://doi.org/10.1016/j.egypro.2015.11.818.
[16] Dostal V, Driscoll M, Hejzlar P. Supercritical CO_2 cycle for fast gas-cooled reactors. Expo 2004;7:683–92. https://doi.org/10.1115/GT2004-54242. Paper No. GT2004-54242.
[17] Moisseytsev A, Sienicki JJ. In: Recent developments in S-CO_2 cycle dynamic modeling and analysis at anl. 4th int symp - supercrit CO_2 power cycles, vol. 53; 2013. p. 1689–99. https://doi.org/10.1017/CBO9781107415324.004.
[18] Turchi CS, Ma Z, Dyreby J. In: Supercritical carbon dioxide power cycle configurations for use in concentrating solar power systems. Vol. 5 manuf. Mater. Metall. Mar. Microturbines small turbomachinery; supercrit. CO_2 power cycles. ASME; 2012. p. 967. https://doi.org/10.1115/GT2012-68932.
[19] Iverson BD, Conboy TM, Pasch JJ, Kruizenga AM. Supercritical CO_2 Brayton cycles for solar-thermal energy. Appl Energy 2013;111:957–70. https://doi.org/10.1016/j.apenergy.2013.06.020.
[20] Singh R, Kearney MP, Manzie C. Extremum-seeking control of a supercritical carbon-dioxide closed Brayton cycle in a direct-heated solar thermal power plant. Energy 2013;60:380–7. https://doi.org/10.1016/j.energy.2013.08.001.
[21] Singh R, Rowlands AS, Miller SA. Effects of relative volume-ratios on dynamic performance of a direct-heated supercritical carbon-dioxide closed Brayton cycle in a solar-thermal power plant. Energy 2013;55:1025–32. https://doi.org/10.1016/j.energy.2013.03.049.
[22] L'Estrange T, Truong E, Rymal C, Rasouli E, Narayanan V, Apte S, et al. High flux microscale solar thermal receiver for supercritical carbon dioxide cycles. In: ASME 2015 13th int. Conf. Nanochannels, microchannels, minichannels. American Society of Mechanical Engineers; 2015. https://doi.org/10.1115/ICNMM2015-48233. V001T03A009.
[23] Silva-Pérez MA. Solar power towers using supercritical CO_2 and supercritical steam cycles, and decoupled combined cycles. Adv Conc Sol Therm Res Technol 2016:383–402. https://doi.org/10.1016/B978-0-08-100516-3.00017-4. Elsevier Inc.
[24] Atif M, Al-Sulaiman FA. Energy and exergy analyses of solar tower power plant driven supercritical carbon dioxide recompression cycles for six different locations. Renew Sustain Energy Rev 2017;68:153–67. https://doi.org/10.1016/j.rser.2016.09.122.
[25] Besarati SM, Goswami DY. Supercritical CO_2 and other advanced power cycles for concentrating solar thermal (CST) systems. Adv Conc Sol Therm Res Technol 2016:157–78. https://doi.org/10.1016/B978-0-08-100516-3.00008-3. Elsevier Inc.
[26] Sabau A, Yin H, Qualls A, McFarlane J. Investigations of supercritical CO_2 Rankine cycles for geothermal power plants. 2011.
[27] McClung A, Brun K, Delimont J. Comparison of supercritical carbon dioxide cycles for oxy-combustion. Vol. 9 oil gas appl. Supercrit. CO_2 power cycles; Wind Energy. ASME; 2015. https://doi.org/10.1115/GT2015-42523.

V009T36A006.
[28] Allam R, Martin S, Forrest B, Fetvedt J, Lu X, Freed D, et al. Demonstration of the allam cycle: an update on the development status of a high efficiency supercritical carbon dioxide power process employing full carbon capture. Energy Procedia 2017;114:5948–66. https://doi.org/10.1016/j.egypro.2017.03.1731.
[29] Huang X, Wang J, Zang J. Thermodynamic analysis of coupling supercritical carbon dioxide brayton cycles 2016;37:34–8. https://doi.org/10.13832/j.jnpe.2016.03.0034.
[30] Wang J, Huang Y, Zang J, Liu G. Preliminary design and considerations of a MWE scale supercritical CO_2 integral test loop. Vol. 9 Oil Gas Appl. Supercrit. CO_2 Power Cycles; Wind Energy, vol. 9. American Society of Mechanical Engineers (ASME); 2016. https://doi.org/10.1115/GT2016-56426. V009T36A002.
[31] Yuansheng L, Jun W, Can M, Chunhui D, Zhenxing Z, Mo T. Design and analysis of key instruments of supercritical carbon dioxide Brayton cycle in future nuclear power field, vol. 2. American Society of Mechanical Engineers (ASME); 2017. https://doi.org/10.1115/ICONE2567155.
[32] Manjunath K, Sharma OP, Tyagi SK, Kaushik SC. Thermodynamic analysis of a supercritical/transcritical CO_2 based waste heat recovery cycle for shipboard power and cooling applications. Energy Convers Manag 2018;155:262–75. https://doi.org/10.1016/j.enconman.2017.10.097.
[33] Sharma OP, Kaushik SC, Manjunath K. Thermodynamic analysis and optimization of a supercritical CO_2 regenerative recompression Brayton cycle coupled with a marine gas turbine for shipboard waste heat recovery. Therm Sci Eng Prog 2017;3:62–74. https://doi.org/10.1016/j.tsep.2017.06.004.
[34] Vesely L, Dostal V. Effect of multicomponent mixtures on cycles with supercritical carbon dioxide. Vol. 9 oil gas appl. Supercrit. CO2 power cycles; wind energy, vol. 9. American Society of Mechanical Engineers (ASME); 2017. https://doi.org/10.1115/GT2017-64044. V009T38A016.
[35] Levy EK, Wang X, Pan C, Romero CE, Maya CR. Use of hot supercritical CO_2 produced from a geothermal reservoir to generate electric power in a gas turbine power generation system. J CO2 Util 2018;23:20–8. https://doi.org/10.1016/j.jcou.2017.11.001.
[36] McClung A, Brun K, Chordia L. Technical and economic evaluation of supercritical oxy-combustion for power generation. Supercrit CO_2 Power 2014:1–14. http://www.sco2symposium.com/www2/sco2/papers2014/systemConcepts/40-McClung.pdf.
[37] Kim MS, Ahn Y, Kim B, Lee JI. Study on the supercritical CO_2 power cycles for landfill gas firing gas turbine bottoming cycle. Energy 2016;111:893–909. https://doi.org/10.1016/j.energy.2016.06.014.
[38] Kacludis A, Lyons S, Nadav D, Zdankiewicz E. Waste heat to power (WH2P) applications using a supercritical CO_2 -based power cycle.
[39] Mondal S, De S. CO_2 based power cycle with multi-stage compression and intercooling for low temperature waste heat recovery. Energy 2015;90:1132–43. https://doi.org/10.1016/j.energy.2015.06.060.
[40] Mohagheghi M, Kapat J. The 4th international symposium -supercritical CO2 power cycles thermodynamic optimization of recuperated S-CO 2 brayton cycles for waste heat recovery applications [n.d].
[41] Moisseytsev A, Sienicki JJ. Investigation of alternative layouts for the supercritical carbon dioxide Brayton cycle for a sodium-cooled fast reactor. Nucl Eng Des 2009;239:1362–71. https://doi.org/10.1016/j.nucengdes.2009.03.017.
[42] Kulhánek M, Dostál V. Supercritical carbon dioxide cycles thermodynamic analysis and comparison. In: Proc SCCO2 Power Cycle Symp; 2011. p. 1–12.
[43] Ahn Y, Bae SJ, Kim M, Cho SK, Baik S, Lee JI, et al. Review of supercritical CO_2 power cycle technology and current status of research and development. Nucl Eng Technol 2015;47:647–61. https://doi.org/10.1016/j.net.2015.06.009.
[44] Crespi F, Gavagnin G, Sánchez D, Martínez GS. Supercritical carbon dioxide cycles for power generation: a review. Appl Energy 2017;195:152–83. https://doi.org/10.1016/J.APENERGY.2017.02.048.
[45] Kimzey G. Development of a Brayton bottoming cycle using supercritical carbon dioxide as the working fluid. EPRI Rep 2012:1–31.
[46] Kim YM, Sohn JL, Yoon ES. Supercritical CO_2 Rankine cycles for waste heat recovery from gas turbine. Energy 2017;118:893–905. https://doi.org/10.1016/j.energy.2016.10.106.
[47] Cho SK, Kim M, Baik S, Ahn Y, Lee JI. Investigation of the bottoming cycle for high efficiency combined cycle gas turbine system with supercritical carbon dioxide power cycle. Vol. 9 oil gas appl. Supercrit. CO_2 power cycles; wind energy. ASME; 2015. https://doi.org/10.1115/GT2015-43077. V009T36A011.
[48] Wright SA, Davidson CS, Scammell WO. Thermo-economic analysis of four sCO_2 waste heat recovery power systems.
[49] Binotti M, Astolfi M, Campanari S, Manzolini G, Silva P. Preliminary Assessment of sCO_2 Power Cycles for Application to CSP Solar Tower Plants. Energy Procedia 2017;105:1116–22. https://doi.org/10.1016/J.EGYPRO.2017.03.475.
[50] Park S, Kim J, Yoon M, Rhim D, Yeom C. Thermodynamic and economic investigation of coal-fired power plant combined with various supercritical CO_2 Brayton power cycle. Appl Therm Eng 2018;130:611–23. https://doi.org/10.1016/J.APPLTHERMALENG.2017.10.145.
[51] Song J, Li X, Ren X, Gu C. Performance analysis and parametric optimization of supercritical carbon dioxide (S-CO_2) cycle with bottoming Organic Rankine Cycle (ORC). Energy 2018;143:406–16. https://doi.org/10.1016/J.ENERGY.2017.10.136.
[52] Mahmoudi S, Akbari A D, Rosen M. Thermoeconomic Analysis and Optimization of a New Combined Supercritical Carbon Dioxide Recompression Brayton/Kalina Cycle. Sustainability 2016;8:1079. https://doi.org/10.3390/su8101079.
[53] NORMALISATION O DE. Systèmes spatiaux–Définition des Niveaux de Maturité de la Technologie (NMT) et de leurs critères d'évaluation. 2013.
[54] Delft TU. Cycle-Tempo™. 2011.
[55] Lemmon EW, Marcia L. Huber and MOM. REFPROP, NIST standard reference database 23, version 8.0. 2007.
[56] Brun K, Friedman P, Dennis R. Fundamentals and applications of supercritical carbon dioxide (sCO_2) based power cycles. Woodhead Publishing an imprint of Elsevier; 2017.
[57] Wang X, Yang Y, Zheng Y, Dai Y. Exergy and exergoeconomic analyses of a supercritical CO_2 cycle for a cogeneration application. Energy 2017;119:971–82. https://doi.org/10.1016/J.ENERGY.2016.11.044.
[58] Laboratories SN. Operation of a Supercritical Fluid Compression Loop Using CO2-Based Mixtures n.d.:2–3.

Nomenclature

Symbols

β: pressure ratio
η: efficiency
h: specific enthalpy [kJ/kg]
$\dot{m}$: mass flow rate [kg/s]
p: pressure [bar]
s: specific entropy [kJ/kgK]
C: cost [$]
CF: cash flow [$]
$\dot{E}$: exergy flow [kW]
$\dot{I}$: irreversibility [kW]
Q: heat load [kJ]
T: temperature [°C]
$\dot{W}$: power [kW]

Subscripts

$_0$: dead state
$_{cs}$: cold side
$_{cum}$: cumulative
$_e$: electrical
$_{ex}$: exergy
$_{hot}$: hot source
$_{hs}$: hot side
$_i$: inlet
$_{inst}$: installation
$_{is}$: isentropic
$_m$: mechanical
$_o$: outlet
$_{rev}$: revenues
$_{tot}$: total
$_{xp}$: expenses
$_C$: compressor
$_{HX}$: heat exchangers
$_T$: turbine

Acronyms

IRR: Internal Rate of Return
LCOE: Levelized Cost Of Electricity
LMTD: Logarithmic Mean Temperature Difference
ORC: Organic Rankine Cycle
PBP: PayBack Period
PH: Pre-Heating
PHPC: Pre-Heating with Pre-Compression
PHSE: Pre-Heating with Split Expansion
PP: Pinch Point
RC: Re-Compression
RCRH: Re-Compression Re-Heating
RH: Re-Heating
SC: Specific Cost
sCO_2: supercritical carbon dioxide
SHSE: Split-Heating with Split Expansion
SR: Simple Regenerated
TIT: Turbine Inlet Temperature
WHR: Waste Heat Recovery